Letter

Experimental test of power-efficiency trade-off in a finite-time Carnot cycle

Ruo-Xun Zhai,[1] Fang-Ming Cui,[1,2] Yu-Han Ma,[1] C. P. Sun,[1,3,*] and Hui Dong[1,†]
[1]*Graduate School of China Academy of Engineering Physics, No. 10 Xibeiwang East Road, Haidian District, Beijing 100193, China*
[2]*Beijing Normal University, Beijing 100875, China*
[3]*Beijing Computational Science Research Center, Beijing 100193, China*

(Received 21 July 2022; revised 6 March 2023; accepted 15 March 2023; published 18 April 2023)

The Carnot cycle is a prototype of an ideal heat engine cycle to draw mechanical energy from the heat flux between two thermal baths with the maximum efficiency, dubbed as the Carnot efficiency η_C. Such efficiency is reached by thermodynamical equilibrium processes with infinite time, accompanied unavoidably with vanishing power-energy output per unit time. The quest to acquire high power leads to an open question of whether a fundamental maximum efficiency exists for finite-time heat engines with given power. We experimentally implement a finite-time Carnot cycle with sealed dry air as a working substance and verify the existence of a trade-off relation between power and efficiency. Efficiency up to $(0.524 \pm 0.034)\eta_C$ is reached for the engine to generate the maximum power, consistent with the theoretical prediction $\eta_C/2$. Our experimental setup shall provide a platform for studying finite-time thermodynamics consisting of nonequilibrium processes.

DOI: 10.1103/PhysRevE.107.L042101

A heat engine converts heat into useful energy, such as mechanical work or electricity. Sadi Carnot derived in 1824 an upper bound $\eta_C = 1 - T_c/T_h$ [1,2] of the conversion efficiency in the Carnot cycle with two isothermal processes for the working substance in two thermal baths with temperatures T_c and T_h and two adiabatic processes. In isothermal processes, a controlled parameter is tuned in a quasi-static fashion—physically much slower than the equilibrium time scale—to reach the Carnot efficiency [2]. Faster processes typically result in more energy dissipation with a consequently lower efficiency, yet can potentially increase the output power [2,3]. Such a trade-off between power and efficiency suggests the possibility of thermodynamically optimizing the two, namely, increasing efficiency while retaining the power or vice versa [4–19]. One might wonder what is the best achievable efficiency, if one exists, for any output power posted by the fundamental laws of thermodynamics [20–26].

Answering such a question requires quantitative evaluations on irreversibility in fundamental nonequilibrium thermodynamics [27,28]. Theoretical models within the near-equilibrium region were explored to reveal a trade-off relation between power and efficiency [20,23,25,29,30] and show the existence of maximum efficiency for any given power. More importantly, a fundamental limit of efficiency with a universal leading order $\eta_C/2$ is predicted for the engine generating the maximum power [15,18,19,21] in various types of finite-time cycles. Aside from the theoretical achievements, it remains with urgency to devise finite-time heat engine cycles to experimentally test these fundamental finite-time thermodynamical constraints [31–35]. The current difficulty to implement the finite-time Carnot cycle is to promptly change the temperature of the thermal bath before and after the adiabatic processes, whose operation time should be far shorter than the equilibrium time to avoid heat exchange [32]. We develop an adiabatic-without-run scheme to implement the finite-time Carnot cycles by separately running only the two finite-time isothermal processes in the high- and low-temperature baths. Such a design is based on the observation that the evaluation of a finite-time Carnot cycle is through two quantities—the heat exchange with a high-temperature bath to evaluate the cycle efficiency and the total work extracted to evaluate the cycle power. The heat exchange can be measured with pressure and volume, and the total work extracted is obtained with the heat exchange difference through the energy conservation law of thermodynamics, without the need to run the two adiabatic processes. With this observation, we can change the bath temperature with the desired accuracy to evaluate the performance of the finite-time Carnot engine. Our scheme allows the essential quantities for evaluating the engine's performance to be obtained from the directly measurable work in the two finite-time isothermal processes with the first law of thermodynamics of energy conservation.

Our experimental verification of the power-efficiency trade-off relation is performed with dry air [36] as a working substance in the finite-time Carnot cycle, which is implemented by changing the volume of the gas $V(t) = V_0 + \mathcal{A}L(t)$ inside a cylindric chamber by moving a piston along a designed path $L(t)$. $\mathcal{A} = \pi d^2/4$ is the area of the chamber's cross section with diameter $d = 5.00$ cm. The chamber is immersed in a water tank as the thermal bath. And the maintenance of the bath temperature (± 0.1 K) is achieved by a feedback temperature control unit. We trace the pressure $p(t)$ with pressure sensors on the chamber, and the piston position $L(t)$ with the stepper motor feedback signal.

*suncp@gscaep.ac.cn
†hdong@gscaep.ac.cn

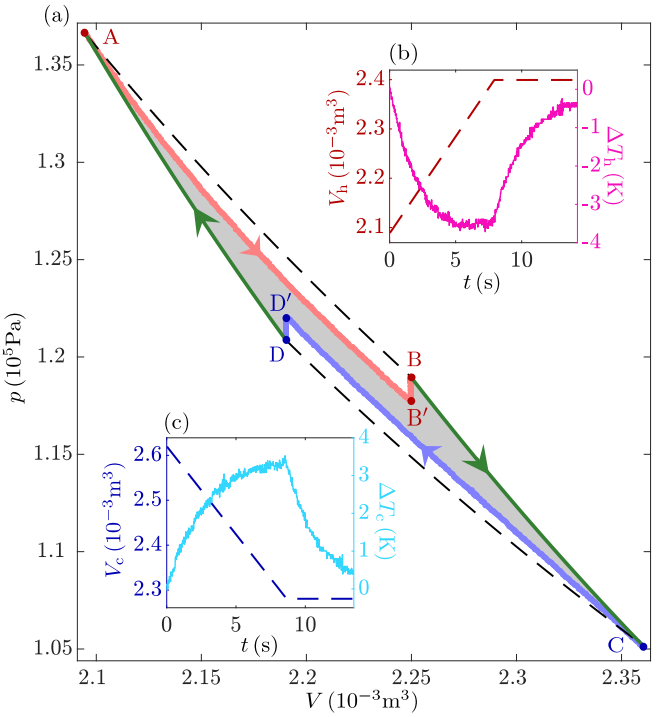

FIG. 1. The finite-time Carnot cycle under the temperature combination $(T_\mathrm{h}, T_\mathrm{c}) = (319.2, 308.2)\,\mathrm{K}$. (a) The Clapeyron pressure-volume (p-V) graph of the finite-time Carnot cycle. The red (upper) and blue (lower) solid lines with arrows show the finite-time isothermal expansion ($A \to B' \to B$) with duration τ_h and compression ($C \to D' \to D$) with duration τ_c, and the green solid lines (left and right) show the adiabatic processes ($B \to C$ and $D \to A$) without actual run. Two relaxation processes ($B' \to B$ and $D' \to D$) with the waiting time $2\tau_\mathrm{relax}$ are added to allow the system to reach equilibrium with the thermal bath. The ideal Carnot cycle ($A \to B \to C \to D$) is presented as gray dashed lines for reference. (b and c) The gaseous volume $V_\mathrm{h(c)}(t)$ (reflected by the dashed line) and the effective temperature trace $\Delta T_\mathrm{h(c)}(t)$ (reflected by the solid line) during the finite-time isothermal expansion and compression. The ideal gas is expanded or compressed with the constant speed $L(t) = L_0 + vt$, with $v_\mathrm{exp} = 20.00\,\mathrm{mm/s}$ and $v_\mathrm{com} = 20.00\,\mathrm{mm/s}$. The total operation time for the example cycle is $t_\mathrm{tot} = 25.92\,\mathrm{s}$.

Our design of the finite-time Carnot cycle is illustrated in Fig. 1(a) with the Clapeyron pressure-volume (p-V) graph composed of two finite-time isothermal processes (upper red and lower blue solid curves) and two no-run adiabatic processes (left and right green solid curves). The graph shows an example run with the temperature combination $(T_\mathrm{h}, T_\mathrm{c}) = (319.2, 308.2)\,\mathrm{K}$. In each run of the finite-time isothermal process, the gas chamber is immersed in the water bath for 10 s to allow the initial equilibration of the gas with the water bath. The gas is expanded [upper red line $A \to B'$ in Fig. 1(a)] or compressed [lower blue line $C \to D'$ in Fig. 1(a)] in the two finite-time isothermal processes with constant speeds controlled by the stepper motor with the precision $\pm 0.02\,\mathrm{mm}$. The pressure traces $p(t)$ measured in the two processes deviate significantly from the equilibrium pressure (dashed black curves) due to the average finite relaxation time $\tau_\mathrm{relax} = 2.77\,\mathrm{s}$. After the expansion and compression, additional waiting time ($2\tau_\mathrm{relax}$) is added to allow the gas to relax to the equilibrium state ($B' \to B$ and $D' \to D$).

TABLE I. Piston positions of finite-time Carnot cycle. Piston positions B and D are calculated with Eq. (1).

T_h(K)	T_c(K)	$\eta_\mathrm{C}(10^{-3})$	Expansion L_B(mm)	Compression L_D(mm)
313.2	311.2	6.39	248.76	17.22
313.2	310.2	9.58	238.22	25.98
314.2	310.2	12.73	227.86	34.72
315.2	310.2	15.87	217.62	43.50
316.2	310.2	18.98	207.49	52.33
317.2	310.2	22.07	197.47	61.20
317.2	309.2	25.22	187.31	70.34
318.2	309.2	28.29	177.48	79.32
319.2	309.2	31.33	167.76	88.34
319.2	308.2	34.47	157.80	97.74

In Figs. 1(b) and 1(c), we show the volume change $V_\mathrm{h(c)}$ (dashed lines) and the effective temperature deviations (solid lines) $\Delta T_\mathrm{h(c)}(t) = T_\mathrm{s}(t) - T_\mathrm{h(c)}$ from the thermal bath temperature $T_\mathrm{h(c)}$. Here, $T_\mathrm{s}(t)$ is the effective gas temperature, which is experimentally estimated by the ideal gas state equation $pV = nRT_\mathrm{s}$ with the amount of substance of gas in moles n and the ideal gas constant R. The gas relaxes to equilibrium with the corresponding thermal bath within the error range determined by the pressure sensors at the end of the relaxation processes ($B' \to B$ and $C' \to C$).

In the adiabatic-without-run scheme, four piston positions (A, B, C, D) are designed for each temperature combination $(T_\mathrm{h}, T_\mathrm{c})$ to ensure the connection between the end (B or D) of one finite-time isothermal process to the beginning (C or A) of the other one with adiabatic processes via the following equations:

$$V_B^{\gamma-1} T_\mathrm{h} = V_C^{\gamma-1} T_\mathrm{c},$$
$$V_D^{\gamma-1} T_\mathrm{c} = V_A^{\gamma-1} T_\mathrm{h}, \qquad (1)$$

where γ is the adiabatic index ($\gamma = 1.40$ for the dry air [37]). The minimum volume V_min is reached at $L_A = 0\,\mathrm{mm}$, and the maximum volume V_C is reached at $L_C = 270.00\,\mathrm{mm}$. The sets of the designed connection points L_i ($i = B, D$) are presented in Table I.

We run the engine cycles with ten temperature combinations to span the Carnot efficiency from $\eta_\mathrm{C} = 6.39\times10^{-3}$ with the temperature combination $(313.2, 311.2)\,\mathrm{K}$ to $\eta_\mathrm{C} = 34.47\times10^{-3}$ with $(319.2, 308.2)\,\mathrm{K}$. For each combination, 27 different values of speeds (v_h and v_c, listed in the Supplemental Material [38]) are chosen to achieve a series of sets of operation time τ_h and τ_c for finite-time isothermal expansion $A \to B' \to B$ and compression processes $C \to D' \to D$.

The heat exchange is obtained with the conservation of energy as $\Delta Q = -W + \Delta U$, where ΔU is the internal energy change of the gas and W is the work performed in each process as $W = -\int p(t)\mathcal{A}dL(t)$. An important property of the ideal gas is that its internal energy depends only on its temperature T_s. The relaxation processes at the end of each finite-time isothermal process ensure the unchanged internal energy $\Delta U_{A\to B} = \Delta U_{C\to D} = 0$, since the gas is

approximately in equilibrium with the water bath $\Delta T_{\mathrm{h(c)}}(t) \approx 0$. The heat absorbed from the high(low)-temperature bath is thus measured directly via

$$Q_{\mathrm{h(c)}} = -W_{\mathrm{h(c)}} = \int_0^{\tau_{\mathrm{h(c)}}} p(t)\mathcal{A}\dot{L}(t)dt. \tag{2}$$

To evaluate the power and efficiency of the current finite-time cycle, we need to determine the total work extracted in the whole cycle. With the law of energy conservation, the total work W_{tot} is measured by the difference of heat exchanges, $W_{\mathrm{tot}} = Q_{\mathrm{h}} + Q_{\mathrm{c}}$. And the power is calculated as the total work extracted during a cycle divided by the total operation time $t_{\mathrm{tot}} = \tau_{\mathrm{h}} + \tau_{\mathrm{c}}$,

$$P(\tau_{\mathrm{h}}, \tau_{\mathrm{c}}) = W_{\mathrm{tot}}/(\tau_{\mathrm{h}} + \tau_{\mathrm{c}}). \tag{3}$$

We remark here that the time for the two adiabatic processes is ignored due to the requirement that the operation time of the adiabatic process should be far shorter than the relaxation time τ_{relax} to avoid heat exchange [15,18]. The efficiency is given by the ratio between the total work W_{tot} and the absorbed heat Q_{h} from the high-temperature thermal bath,

$$\eta(\tau_{\mathrm{h}}, \tau_{\mathrm{c}}) = W_{\mathrm{tot}}/Q_{\mathrm{h}}. \tag{4}$$

In Fig. 2(a), we show the plot of the power $P(\tau_{\mathrm{h}}, \tau_{\mathrm{c}}) = W_{\mathrm{tot}}/t_{\mathrm{tot}}$ as the function of the two operation times τ_{h} and τ_{c} for cycles under the temperature combination $(T_{\mathrm{h}}, T_{\mathrm{c}}) = (319.2, 308.2)\,\mathrm{K}$. The competition between the increase of total work W_{tot} (equal to the gray area enclosed by the p-V curve) and the increase of total operation time τ_{tot} results in a point of maximum power $P_{\mathrm{max}} = 0.030\,\mathrm{J/s}$ on the power surface with the optimal operation time $\tau_{\mathrm{h}}^* = 13.32\,\mathrm{s}$ and $\tau_{\mathrm{c}}^* = 12.60\,\mathrm{s}$ [red arrow in Fig. 2(a)].

Recently, much theoretical attention has been drawn to finding the trade-off between power and efficiency for finite-time thermodynamic cycles [15,32]. Within the framework of the low-dissipation model [15,18], a power and efficiency trade-off relation [20,23,25] is predicted for the finite-time Carnot cycle.

In Fig. 2(b), we show the scatter plot of the normalized efficiency η/η_{C} and the normalized output power P/P_{max} for cycles with different operation times τ_{h} and τ_{c}. The error bars of each set P and η are obtained from eight repeats of each experimental run. The dashed red line shows the theoretical constraint [25] between the normalized efficiency $\widetilde{\eta} \equiv \eta/\eta_{\mathrm{C}}$ and power $\widetilde{P} \equiv P/P_{\mathrm{max}}$ with the upper bound $\widetilde{\eta} \leqslant 1 - (1-\eta_{\mathrm{C}})\widetilde{P}/[2(1+\sqrt{1-\widetilde{P}}) - \eta_{\mathrm{C}}\widetilde{P}]$ and the lower bound $\widetilde{\eta} \geqslant (1-\sqrt{1-\widetilde{P}})/2$. The red shadow region represents the uncertainty of the constraint caused by the temperature fluctuations of the water bath. The experimental data (colored circles) fall into the region enclosed by the two margins of the upper and lower bound in Fig. 2(b). The data illustrates not only an upper bound for the achievable efficiency for the given power, but also a lower bound for the worst efficiency for the current finite-time Carnot cycle. The Carnot efficiency $\eta_{\mathrm{C}} = 34.47\times10^{-3}$ is achieved with the increasing operation time τ_{c} and τ_{h} at the top left corner with the vanishing power. Similar plots for other temperature combinations are illustrated in the Supplemental Material [38].

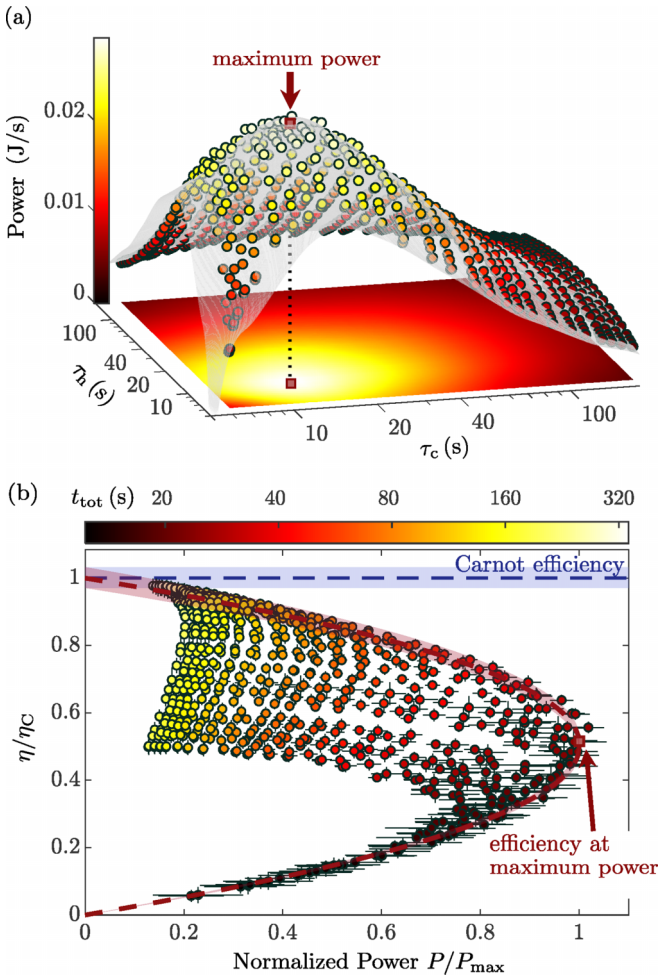

FIG. 2. Power and efficiency of the finite-time Carnot engine under the temperature combination $(T_{\mathrm{h}}, T_{\mathrm{c}}) = (319.2, 308.2)\,\mathrm{K}$. (a) Output power $P(\tau_{\mathrm{h}}, \tau_{\mathrm{c}})$ as a function of operation time $(\tau_{\mathrm{h}}, \tau_{\mathrm{c}})$. Each circle shows the output power averaged over eight repeats of the measurement. The arrow shows the position of the maximum power with the control time $\tau_{\mathrm{h}}^* = 13.32\,\mathrm{s}$ and $\tau_{\mathrm{c}}^* = 12.60\,\mathrm{s}$. (b) Efficiency-power trade-off (circles with error bar). The dashed blue line (upper) shows the Carnot efficiency $\eta_{\mathrm{C}} = 34.47\times10^{-3}$, and the blue shadow presents the efficiency fluctuation due to temperature variation of the water bath during the experiments. The total time of the cycle is shown with colors.

The key quantity to evaluate the finite-time Carnot cycle is the efficiency at the maximum power η_{EMP}, which was suggested to have an upper limit independent of the properties of the working substance [7,18]. We extract the efficiency at the maximum power η_{EMP} for all the temperature combinations in our experiment, and show its dependence on the Carnot efficiency in Fig. 3(a). The obtained maximum efficiencies (markers with error bars) follow a simple relation $\eta_{\mathrm{EMP}} = (0.524 \pm 0.034)\eta_{\mathrm{C}}$. It agrees well with the efficiency at maximum power of various models of finite-time cycles to the first order of the Carnot efficiency η_{C} as $\eta_{\mathrm{EMP}}^{\mathrm{th}} = \eta_{\mathrm{C}}/2 + \mathcal{O}(\eta_{\mathrm{C}}^2)$, for example, in the Curzon-Ahlborn model [7] $\eta_{\mathrm{CA}} = 1 - \sqrt{1-\eta_{\mathrm{C}}}$, in the recent proposed bound of stochastic engines [16,18] $\eta_{\mathrm{C}}/(2-\eta_{\mathrm{C}})$, and in the Feynman ratchets $\eta_{\mathrm{C}}^2/[\eta_{\mathrm{C}} - (1-\eta_{\mathrm{C}})\ln(1-\eta_{\mathrm{C}})]$ [19]. The coefficient 1/2 was

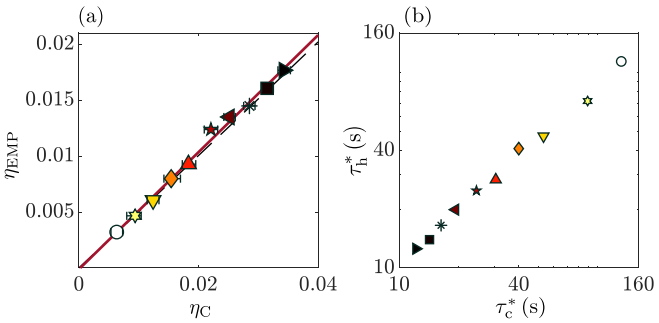

FIG. 3. Optimized finite-time Carnot cycle with maximum power. (a) Efficiency at maximum power (markers with error bars) as a function of Carnot efficiency. The red solid line shows the linear fit $\eta_{\rm EMP} = a + b\eta_{\rm C}$ yielding the parameters $a = \pm 7.0\times10^{-4}$ and $b = 0.524 \pm 0.034$. The dashed black line shows the Curzon-Ahlborn efficiency $\eta_{\rm CA} = 1 - \sqrt{1-\eta_{\rm C}}$. (b) Optimal operation time $(\tau_{\rm h}^*, \tau_{\rm c}^*)$ for the maximum power in the cycles with different Carnot efficiencies. The same symbols in (a) and (b) correspond to the same experimental data set.

proved as a universal value independent of the system-specific features in the linear response regime due to the symmetry of the Onsager relations [15,28]. Our experimental data provide a demonstration of the leading order with the coefficient $1/2$.

Optimization of the cycle for maximum power is achieved by choosing the operation time $\tau_{\rm h}$ and $\tau_{\rm c}$. We determine the corresponding optimal operation time $(\tau_{\rm h}^*, \tau_{\rm c}^*)$, illustrated as markers in Fig. 3(b). The same symbols in (a) and (b) correspond to the same experimental data set. The optimal operation time $(\tau_{\rm h}^*, \tau_{\rm c}^*)$ is verified to be in the regime where the $1/\tau$ scaling is valid [32,36] (discussion in the Supplemental Material [38]). For higher Carnot efficiency, less optimal operation time is needed to achieve the maximum power, and in turn more irreversibility is generated.

In summary, we have experimentally implemented the finite-time Carnot cycle with dry air as the working substance. For any given output power, we have shown the existence of the highest efficiency achieved with the designed operation time, which is in agreement with the theoretical prediction of power-efficiency constraint relations. Our results also verify the theoretically predicted universal relation of the efficiency at maximum power $\eta_{\rm EMP} = \eta_{\rm C}/2 + \mathcal{O}(\eta_{\rm C}^2)$ to the first order of the Carnot efficiency as $\eta_{\rm EMP} = (0.524 \pm 0.034)\eta_{\rm C}$. We believe that the current setup will provide an ideal platform for testing the finite-time thermodynamics predictions and also spur more experimental efforts into exploring the finite-time thermodynamics.

This work is supported by the National Natural Science Foundation of China (NSFC) (Grants No. 12088101, No. 11534002, No. 11875049, No. U1930402, No. U1930403, and No. 12047549) and the National Basic Research Program of China (Grant No. 2016YFA0301201).

[1] S. Carnot, in *Reflections on the Motive Power of Heat and on Machines Fitted to Develop that Power*, edited by R. H. Thurston (Wiley, New York, 1890).
[2] H. B. Callen, *Thermodynamics and an Introduction to Thermostatistics* (John Wiley & Sons, New York, 1985).
[3] B. Andresen, P. Salamon, and R. S. Berry, Thermodynamics in finite time, Phys. Today **37**, 62 (1984).
[4] J. Yvon, The Saclay reactor: Two years experience on heat transfer by means of a compressed gas, in *Proceedings of the International Conference on Peaceful Uses of Atomic Energy* (Geneva, 1955), p. 387.
[5] P. Chambadal, *Les Centrales Nucléaires* (Armand Colin, Paris, 1957).
[6] I. Novikov, The efficiency of atomic power stations, J. Nucl. Energy (1954) **7**, 125 (1958).
[7] F. L. Curzon and B. Ahlborn, Efficiency of a Carnot engine at maximum power output, Am. J. Phys. **43**, 22 (1975).
[8] B. Andresen, R. S. Berry, A. Nitzan, and P. Salamon, Thermodynamics in finite time. I. The step-Carnot cycle, Phys. Rev. A **15**, 2086 (1977).
[9] M. H. Rubin, Figures of merit for energy conversion processes, Am. J. Phys. **46**, 637 (1978).
[10] P. Salamon, A. Nitzan, B. Andresen, and R. S. Berry, Minimum entropy production and the optimization of heat engines, Phys. Rev. A **21**, 2115 (1980).
[11] A. D. Vos, Efficiency of some heat engines at maximum-power conditions, Am. J. Phys. **53**, 570 (1985).
[12] R. D. Spence and M. J. Harrison, Speed dependence of the efficiency of heat engines, Am. J. Phys. **53**, 890 (1985).
[13] H. S. Leff, Thermal efficiency at maximum work output: New results for old heat engines, Am. J. Phys. **55**, 602 (1987).
[14] A. Bejan, Models of power plants that generate minimum entropy while operating at maximum power, Am. J. Phys. **64**, 1054 (1996).
[15] C. Van den Broeck, Introduction to Thermodynamics of Irreversible Processes, Phys. Rev. Lett. **95**, 190602 (2005).
[16] T. Schmiedl and U. Seifert, Efficiency at maximum power: An analytically solvable model for stochastic heat engines, Europhys. Lett. **81**, 20003 (2007).
[17] B. H. Lavenda, The thermodynamics of endoreversible engines, Am. J. Phys. **75**, 169 (2007).
[18] M. Esposito, R. Kawai, K. Lindenberg, and C. Van den Broeck, Efficiency at Maximum Power of Low-Dissipation Carnot Engines, Phys. Rev. Lett. **105**, 150603 (2010).
[19] Z. C. Tu, Efficiency at maximum power of Feynman's ratchet as a heat engine, J. Phys. A: Math. Theor. **41**, 312003 (2008).
[20] A. Ryabov and V. Holubec, Maximum efficiency of steady-state heat engines at arbitrary power, Phys. Rev. E **93**, 050101(R) (2016).
[21] V. Holubec and A. Ryabov, Maximum efficiency of low-dissipation heat engines at arbitrary power, J. Stat. Mech. (2016) 073204.
[22] R. Long and W. Liu, Efficiency and its bounds of minimally nonlinear irreversible heat engines at arbitrary power, Phys. Rev. E **94**, 052114 (2016).
[23] N. Shiraishi, K. Saito, and H. Tasaki, Universal Trade-Off Relation between Power and Efficiency for Heat Engines, Phys. Rev. Lett. **117**, 190601 (2016).
[24] V. Cavina, A. Mari, and V. Giovannetti, Slow Dynamics and Thermodynamics of Open Quantum Systems, Phys. Rev. Lett. **119**, 050601 (2017).

[25] Y.-H. Ma, D. Xu, H. Dong, and C.-P. Sun, Universal constraint for efficiency and power of a low-dissipation heat engine, Phys. Rev. E **98**, 042112 (2018).

[26] P. Abiuso and M. Perarnau-Llobet, Optimal Cycles for Low-Dissipation Heat Engines, Phys. Rev. Lett. **124**, 110606 (2020).

[27] I. Prigogine, *Introduction to the Thermodynamics of Irreversible Processes*, 3rd ed. (Wiley, New York, 1968).

[28] U. Seifert, Stochastic thermodynamics, fluctuation theorems and molecular machines, Rep. Prog. Phys. **75**, 126001 (2012).

[29] L. Chen and Z. Yan, The effect of heat-transfer law on performance of a two-heat-source endoreversible cycle, J. Chem. Phys. **90**, 3740 (1989).

[30] Y. H. Chen, J.-F. Chen, Z. Fei, and H. T. Quan, Microscopic theory of the Curzon-Ahlborn heat engine based on a Brownian particle, Phys. Rev. E **106**, 024105 (2022).

[31] V. Blickle and C. Bechinger, Realization of a micrometre-sized stochastic heat engine, Nat. Phys. **8**, 143 (2011).

[32] I. A. Martínez, É. Roldán, L. Dinis, D. Petrov, J. M. R. Parrondo, and R. A. Rica, Brownian Carnot engine, Nat. Phys. **12**, 67 (2015).

[33] J. Rossnagel, S. T. Dawkins, K. N. Tolazzi, O. Abah, E. Lutz, F. Schmidt-Kaler, and K. Singer, A single-atom heat engine, Science **352**, 325 (2016).

[34] M. Josefsson, A. Svilans, A. M. Burke, E. A. Hoffmann, S. Fahlvik, C. Thelander, M. Leijnse, and H. Linke, A quantum-dot heat engine operating close to the thermodynamic efficiency limits, Nat. Nanotechnol. **13**, 920 (2018).

[35] M. Josefsson, A. Svilans, H. Linke, and M. Leijnse, Optimal power and efficiency of single quantum dot heat engines: Theory and experiment, Phys. Rev. B **99**, 235432 (2019).

[36] Y.-H. Ma, R.-X. Zhai, J. Chen, C. P. Sun, and H. Dong, Experimental Test of the 1/t-Scaling Entropy Generation in Finite-Time Thermodynamics, Phys. Rev. Lett. **125**, 210601 (2020).

[37] D. E. Krause and W. J. Keeley, Determining the heat capacity ratio of air from almost adiabatic compressions, Phys. Teach. **42**, 481 (2004).

[38] See Supplemental Material at http://link.aps.org/supplemental/10.1103/PhysRevE.107.L042101 for detailed discussion on apparatus calibration, cycle design, and data processing.